Ocean Engineering 350 (2026) 124258

Contents lists available at ScienceDirect

Ocean Engineering

journal homepage: www.elsevier.com/locate/oceaneng

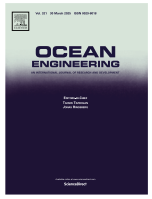

Design loads assessment for FOWT in the Mediterranean sea: a comparative analysis between alternative approaches

Elisa Marchelli [a,*], Francesco De Leo [b], Giovanni Besio [b], Cesare Mario Rizzo [a]

[a] University of Genoa, Electrical, Electronic, Telecommunications Engineering and Naval Architecture Department, Genoa, 16145, Italy
[b] University of Genoa, Civil, Chemical and Environmental Engineering Department, Genoa, 16145, Italy

ARTICLE INFO

Keywords:
Floating offshore wind turbines
Environmental contours
IFORM
Mediterranean sea

ABSTRACT

Existing guidelines recommend the use of the Environmental Contours method to estimate site-specific extreme environmental conditions, which critically influence both the operational efficiency and structural integrity of Floating Offshore Wind Turbines (FOWTs). While different approaches for computing such contours have been proposed in previous literature, the major source of uncertainty is still represented by the extreme data selection. In this respect, this study extracts Environmental Contour surfaces at four locations in the Mediterranean Sea relying on three different approaches, i.e., annual maxima, peak over threshold, and complete dataset, for environmental parameters representing the primary loading sources, namely hourly mean wind speed (U_w), significant wave height (H_s), and peak period (T_p). Results across all sites indicate that H_s peaks on the contour surfaces are overestimated when using the entire dataset compared to selecting only extreme values, underscoring the influence of the marginal distribution on environmental contour computations. Finally, the comparison of excitation levels across different sites supports the calibration of FOWT designs specifically for the Mediterranean Sea, as existing design criteria and recommendations are primarily tailored to the more severe conditions of the North Sea and the Atlantic Ocean. This approach offers potential cost-reduction benefits, aiding decision-making in a region with a high demand for renewable energy.

1. Introduction

Offshore wind technology has been identified as a potentially effective means of producing renewable energy, aligning with sustainability and decarbonization targets to alleviate climate change. By 2030, the European Union aims to reach 425 GW of installed wind capacity, almost doubling the 2023 production of 220 GW, of which 201 GW onshore and 19 GW offshore. The outlook consists of an expansion in offshore wind capacity, with annual offshore installations expected to outgrow the onshore towards the end of the decade (Windeurope, 2025). The expansion of this market is expected to benefit especially from Floating Offshore Wind Turbines (FOWTs), which offer a cost-competitive solution for deep waters, i.e. over 50 m water depth, allowing installations further from the coasts compared to traditional fixed bottom technologies. This makes FOWT particularly convenient in the Mediterranean basin, where coastal areas often host protected cultural heritage sites which may conflict with such developments. In this respect, semi-submersible platforms have shown promising performances in the area, with hotspots identified based on levelized cost of energy (LCOE) and benefitting from optimal wind regimes (Martinez and Iglesias, 2021).

Currently, guidelines for the design of FOWTs present a variety of alternatives, with several criteria adapted from the oil and gas industry. DNV and International Electrotechnical Commission (IEC) guidelines specifically address the design of FOWTs adopting the Limit State approach. The standards require that the extreme response corresponding to a return period be determined by applying site-specific environmental loads to the structure. Although the full long-term analysis approach can accurately predict the structural response considering all sea states (Soares, 1993), the Environmental Contour (EC) method offers an efficient and more doable alternative. By extracting a reduced sub-sets of relevant forcing, this allows to reduce the computational load particularly during the preliminary design stages, while complying with most design guidelines.

In this framework, one well established tool is the inverse-first order reliability method (IFORM) (Winterstein et al., 1993), which paved the road for numerous works on the topic.

Alternative approaches have also been developed for the computation of ECs. Haselsteiner et al. (2017) leads to similar contours to the IFORM ones but associated to lower probability levels and therefore being hardly comparable, Silva-González et al. (2013) used a Nataf

* Corresponding author.
E-mail addresses: elisa.marchelli@edu.unige.it (E. Marchelli), elisa.marchelli@edu.unige.it (C.M. Rizzo).

https://doi.org/10.1016/j.oceaneng.2026.124258
Received 26 March 2025; Received in revised form 12 July 2025; Accepted 7 January 2026

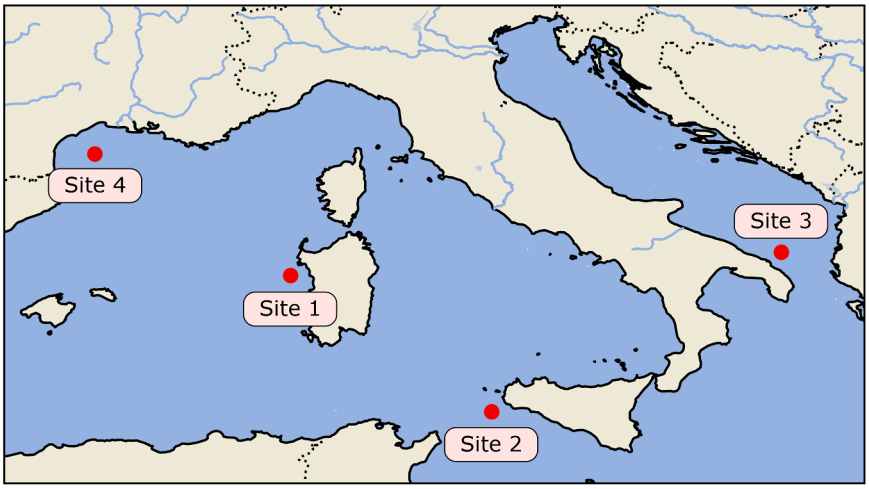

Fig. 1. Locations of the potential offshore installation sites of semi-submersible FOWTs in the MS (Met Office, 2010).

transformation which implies that Gaussian (thus symmetric) Copulas define the joint density of the variables, an assumption often too strict in case of metocean scatters. Huseby et al. (2015) introduced a new method based on Monte Carlo bootstrap that yield very similar results to the IFORM for convex contours (Vanem and Bitner-Gregersen, 2015). Neither method requires massive computational costs for the extrapolation of the EC, so the available resources do not affect the choice. In view of the above, the IFORM method is applied in the present study, given its well-established robustness, ease of implementation, and widespread use within the scientific community.

At present, limited research has explored how reduced environmental conditions should be selected to reduce the computational cost for the structural assessment of a FOWT (Li et al., 2024; Li and Zhang, 2020; Wang and Moan, 2023, 2024). Additionally, a few applications have been presented to date in the Mediterranean Sea (MS; see, e.g., Leo et al., 2021; Mikulić and Parunov, 2023), and existing guidelines, developed in the North European regions, have yet to be tailored for applications in the Mediterranean region. This is relevant considering that most current standards have been formulated based on the metocean conditions typical of Northern Europe, which may not accurately reflect the environmental characteristics of other regions characterized by milder climates, such as the Mediterranean Sea, potentially leading to overly conservative design. The MS is indeed an enclosed basin, implying that waves are mostly locally generated and are associated with lower amplitudes and shorter periods (compare in this respect, e.g., the wind and wave maps in Chirosca and Rusu, 2022), owing to limited fetches and exposure to rough atmospheric patterns (Barbariol et al., 2021).

Based on the above grounds, in this work we apply the IFORM approach to derive EC surfaces representing the combined wind and wave parameters at four test sites in the MS. Analysis are based on hindcast data reconstructed in the 1979-2020 period. Long-term joint distributions of the mean wind speed at 10 m height (U_w), significant wave height (H_s), and spectral peak period (T_p) are modeled through EC surfaces resulting from different data selection. Namely, the probability of occurrence of Annual Maxima (AM) and independent storms identified using the Peak-Over-Threshold method (POT) are discussed, and next the results obtained from both approaches are compared with those stemming from the complete data sets (that is the initial distribution approach or ID selection) (Velarde et al., 2019). From a theoretical point of view, the POT approach is expected to outperform the AM as it retains a higher number of peaks, thereby improving the fitting of the probability distribution subsequently used to model the extremes. However, the selection of the threshold does not come with ease (Lang et al., 1999) and can introduce additional uncertainty into the analysis. On the other hand, the ID does not require subjective thresholds selection but it violates the assumption of independent and Identically Distributed data. Moreover, probability distributions often fail to capture the behavior of the data tails, being biased toward the bulk of the data around the mode (Vanem, 2015). The use of different approaches in extreme value analysis has long been discussed in the literature and still represents an open question, as different choices can affect the extrapolated extremes to a great extent. While previous literature has primarily focused on comparing predictions of the marginal distributions corresponding to the approaches above (Bezak and Šraj, 2014; Teena et al., 2012; Volpi et al., 2019), the following study extends the analysis to understand their influence on the EC assessment. This enables an investigation of the EC surface region associated with the highest H_s, which is critical for identifying design states relevant to FOWT excitation.

Starting from the ECs, the purpose of the study is to provide a set of environmental loads following the methodology proposed in Wang and Moan (2024) for the Ultimate Limit State (ULS), according to the current guidelines. To this end, the Response Amplitude Operators (RAOs) of a typical FOWT with a semi-submersible platform (Coulling et al., 2013; Tran and Kim, 2015; Wang et al., 2023) are employed, allowing to detect crucial design combinations. Although the reference structures are designed to accommodate wind turbines in Northern European regions, their dynamic characteristics are deemed relevant to assess how Mediterranean conditions reflect on the loading of commercially available systems.

The article is organized as follows. After this Introduction, Section 2 details the methodology used to assess the EC surfaces, subsequently used for selecting the design states according to the ULS for the structure. Section 3 introduces the case studies including the data used, while Section 4 presents and discusses the results, followed by Section 5, which draws the conclusions of this research.

2. Methodology

This section details the methodology for a comparative analysis of the EC surfaces for the four selected sites, and the dynamic characteristics of a semi-semisubmersible FOWT based on its typical RAOs. The development of the EC is based on a joint environmental model for wind and wave conditions, achieved by fitting analytical formulations to the relevant metocean variables. In this study, the hierarchical conditional model factorizes the joint Probability Density Function (PDF) into the product of the PDFs of the single variables. The hierarchical conditional model relies on predefined assumptions regarding the distributional form of each variable, where the parameters of one variable's distribution are expressed conditionally on others through a specified

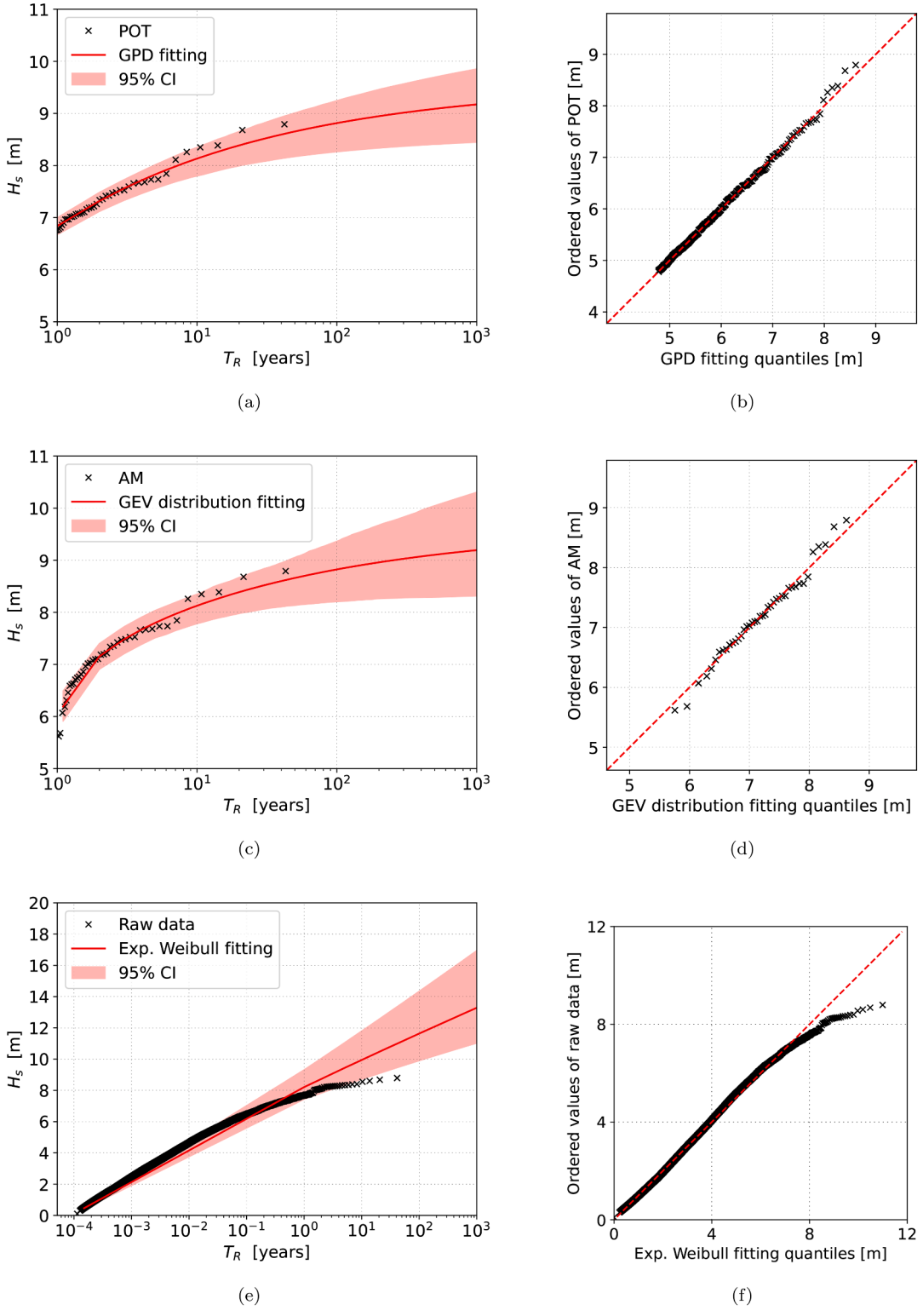

Fig. 2. Inverse marginal CDF and qqplot of the POT (a)(b), the AM (c)(d) and the complete set of raw data (e)(f) of H_s.

parametric dependence structure. This approach typically involves fitting the model to the full dataset, implicitly assuming that the observations are independent and identically distributed (Hauteclocque et al., 2022). The joint PDF is expressed as follows:

$$f_{H_s,T_p,U_w}(h,t,u) = f_{H_s}(h) f_{U_w|H_s}(u|h) f_{T_p|H_s,U_w}(t|h,u) \tag{1}$$

where H_s, U_w and T_p indicate random variables, while h, u and t represent their realizations. The PDFs factorizing the joint distribution model are respectively: the marginal PDF of H_s, $f_{H_s}(h)$, the conditional PDF of U_w given H_s, $f_{U_w|H_s}(u|h)$, and the conditional distribution of T_p given H_s and U_w, $f_{T_p|H_s,U_w}(t|h,u)$ (Haselsteiner et al., 2020).

The marginal distribution of H_s is the only distinguishing factor in generating the joint distributions for AM, POT, and the complete raw

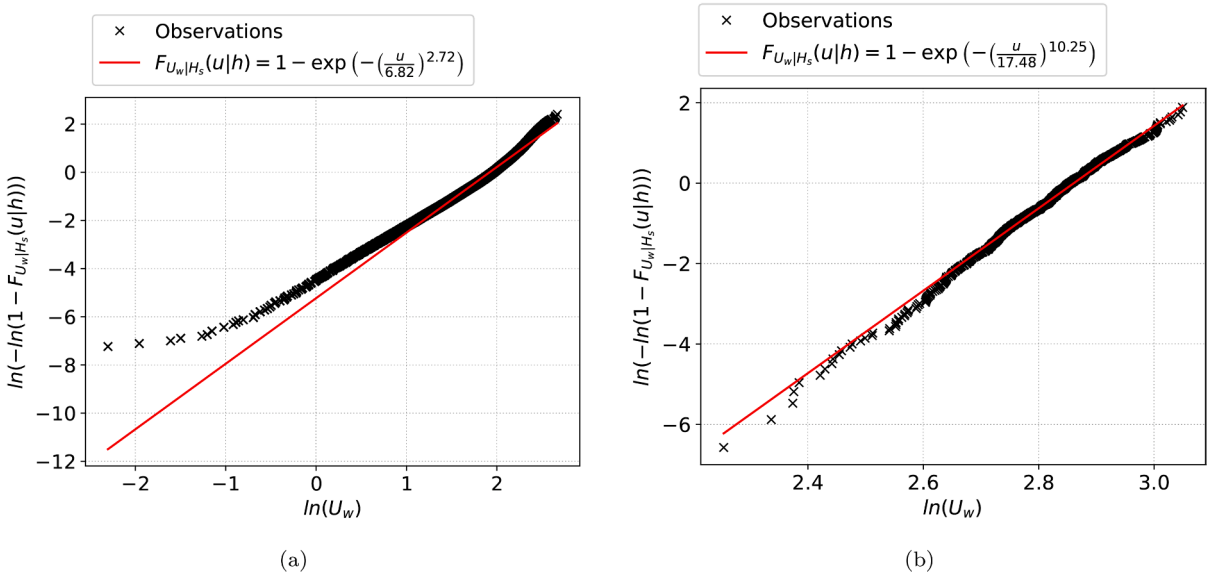

Fig. 3. Cumulative distribution of U_w within different H_s classes. The empirical observations are given together with the fitted Weibull distribution. (a) $1.0 \leq H_s \leq 1.5$ and (b) $5.5 \leq H_s \leq 6.0$.

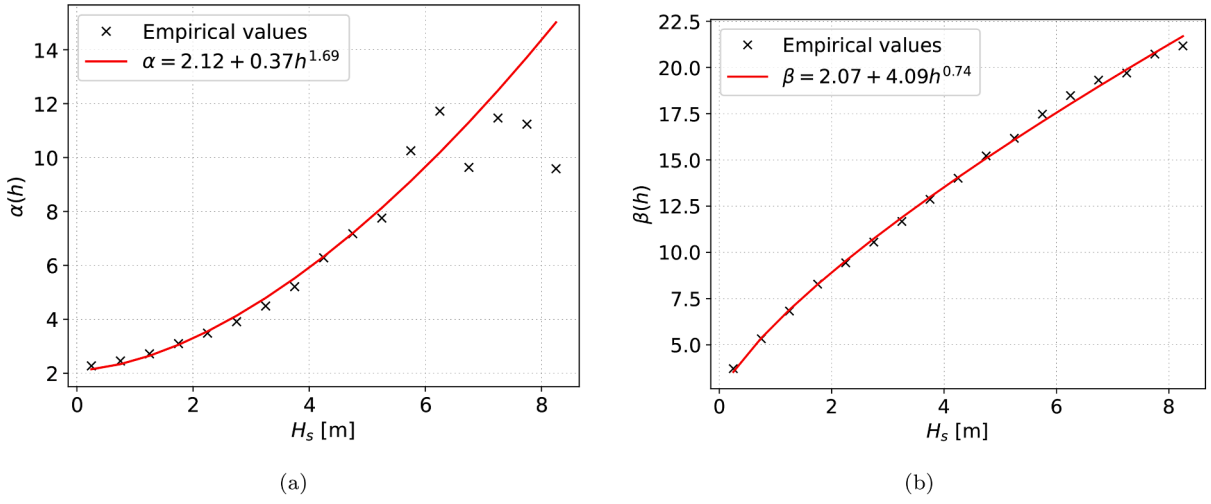

Fig. 4. Proposed models of (a) $\alpha(h)$ and (b) $\beta(h)$, along with empirical values for the H_s classes.

data sets. In this research, we use the Generalized Extreme Value (GEV) and Generalized Pareto Distribution (GPD) for AM and POT series of H_s, respectively (note that these are the classical distributions used for such subsets; Coles et al., 2001). In the POT method, the peak excesses above a high threshold – set in this study as the 99th percentile of the empirical distribution of H_s – are assumed to occur as stochastically independent events, considering a minimum time lag of 24 hours between consecutive peaks (Ferreira and Soares, 1998; Goda, 2000; Luceño et al., 2006; Soukissian et al., 2006; Zachary et al., 1998).

As for the entire data set, we rely on the exponentiated Weibull distribution (Haselsteiner and Thoben, 2020), whose PDF reads:

$$f_{H_s}(h) = \alpha \frac{k}{\lambda}\left(\frac{h}{\lambda}\right)^{k-1}\left[1 - \exp\left(-\frac{h}{\lambda}\right)^{k}\right]^{\alpha-1}\exp\left(-\frac{h}{\lambda}\right)^{k} \tag{2}$$

where k is the first shape parameter, α is the second shape parameter and λ is the scale parameter of the distribution.

The conditional distribution of U_w given H_s is modeled through a Weibull distribution (Morgan et al., 2011):

$$f_{U_w|H_s}(u|h) = \begin{cases} \frac{\alpha(h)}{\beta(h)}\left(\frac{u}{\beta(h)}\right)^{\alpha(h)-1}\exp\left[-\left(\frac{u}{\beta(h)}\right)^{\alpha(h)}\right], & u \geq 0 \\ 0, & u < 0 \end{cases} \tag{3}$$

The Weibull shape and scale parameters, $\alpha(h)$ and $\beta(h)$ are estimated by grouping U_w data into H_s classes, and next fitting the following functions:

$$\alpha(h) = a_1 + a_2 h^{a_3}, \qquad \beta(h) = b_1 + b_2 h^{b_3} \tag{4}$$

where a_1, a_2, a_3, b_1, b_2 and b_3 are tuning parameters.

The lognormal distribution is employed to model the conditional distribution of T_p given H_s and U_w, estimated using the procedure outlined in Johannessen et al. (2002). The corresponding PDF is expressed as:

$$f_{T_p|H_s,U_w}(t|h,u) = \frac{1}{\sqrt{2\pi}\sigma_{\ln(T_p)}(h,u)t}\exp\left[-\frac{1}{2}\left(\frac{\ln(t) - \mu_{\ln(T_p)}(h,u)}{\sigma_{\ln(T_p)}(h,u)}\right)^2\right] \tag{5}$$

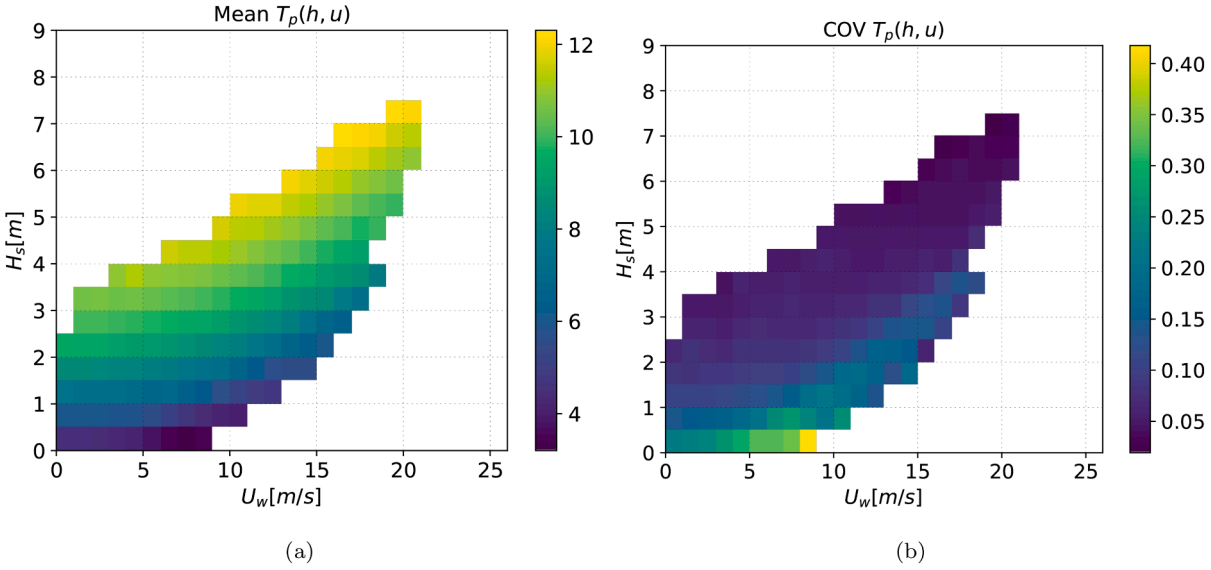

(a) (b)

Fig. 5. Empirical values of (a) $\mu_{T_p}(h,u)$ and (b) $\nu_{T_p}(h,u)$ within each wind-wave class.

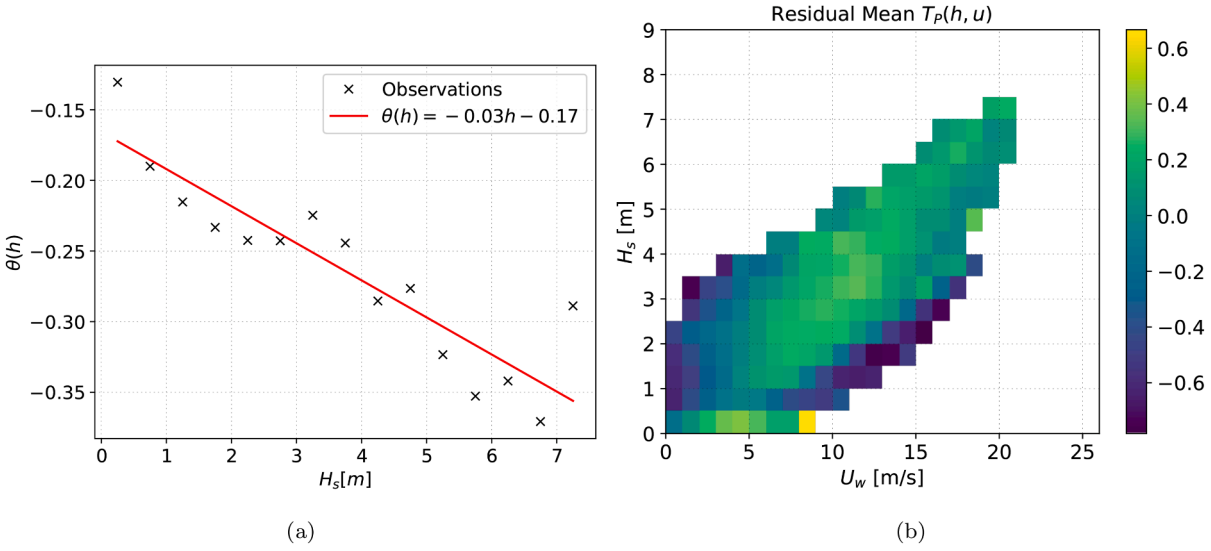

(a) (b)

Fig. 6. (a) The slope $\theta(h)$ between the normalized T_p and the normalized wind speed, as function of H_s and, (b) the residuals between empirical mean T_p and proposed model $\mu_{T_p}(h,u)$ across the wind-wave classes. Positive residuals indicate that the empirical mean T_p exceeds the values predicted by the model.

The parameters $\mu_{ln(T_p)}(h,u)$ and $\sigma_{ln(T_p)}(h,u)$, representing the mean and standard deviation of $\ln(T_p)$, are expressed as functions of the mean and standard deviation of T_p, denoted as $\mu_{T_p}(h,u)$ and $\sigma_{T_p}(h,u)$, respectively. The following formulation is adopted to incorporate conditionality:

$$\mu_{\ln(T_p)}(h,u) = \ln\left(\frac{\mu_{T_p}(h,u)}{\sqrt{1+\nu^2_{T_p}(h,u)}}\right), \qquad \sigma^2_{\ln(T_p)}(h,u) = \ln\left(\nu^2_{T_p}(h,u)+1\right) \quad (6)$$

where

$$\nu_{T_p}(h,u) = \frac{\sigma_{T_p}(h,u)}{\mu_{T_p}(h,u)} \quad (7)$$

The parameter $\mu_{ln(T_p)}(h,u)$ can be represented as a function of the expected spectral peak period $\bar{t}(h)$ and mean wind speed $\bar{u}(h)$, with fitting coefficients θ and γ:

$$\mu_{T_p}(h,u) = \bar{t}(u,h) = \bar{t}(h)\left[1+\theta\left(\frac{u-\bar{u}(h)}{\bar{u}(h)}\right)^{\gamma}\right] \quad (8)$$

where

$$\bar{t}(h) = e_1 + e_2 h^{e_3}, \qquad \bar{u}(h) = f_1 + f_2 h^{f_3} \quad (9)$$

being e_1, e_2, e_3, f_1, f_2 and f_3 parameters to be estimated from the data. The expression $[1+\theta(u-\bar{u}(h)/\bar{u}(h)^{\gamma}]$ adjusts the expected T_p, based on the offset between actual and expected wind speeds for a given H_s value. For improved parameter estimation, $\theta(h)$ and γ can be derived by rewriting the Eq. 8 as:

$$\frac{\bar{t}(u,h)-\bar{t}(h)}{\bar{t}(h)} = \theta\left(\frac{u-\bar{u}(h)}{\bar{u}(h)}\right)^{\gamma} \quad (10)$$

A linear relation between $\theta(h)$ and the H_s classes is adopted:

$$\theta(h) = m_1 + m_2 h \quad (11)$$

For the sake of simplicity, $\nu_{T_p}(h)$ can be assumed to be a function of H_s alone:

$$\nu_{T_p}(h) = k_1 + k_2 \exp(hk_3) \quad (12)$$

The Maximum Likelihood method (MLM) is used to estimate the fitting parameters of the GEV and the GP distributions, while the Linear

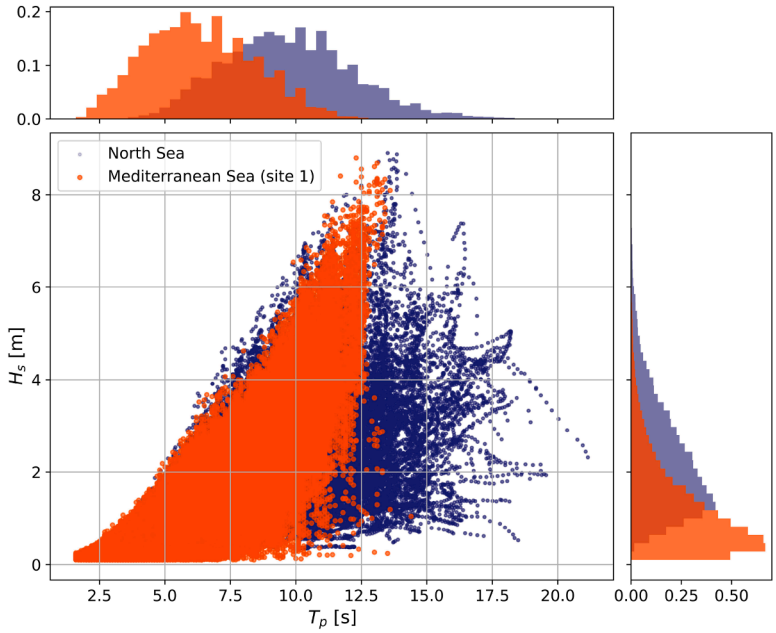

Fig. 7. H_s-T_p observations at two locations: one in the Mediterranean Sea (site 1) and one in the North Sea, with corresponding marginal histograms.

Least Squared (LLS) method prioritizing high quantiles of H_s is applied for the exponentiated Weibull distribution (Haselsteiner and Thoben, 2020). The Non-Linear Least Squares (NLS) method is used to assess the conditional distributions' fitting parameters (Pfanzagl, 1994).

The estimation of wind and sea state conditions corresponding to a specified return period is performed using the IFORM approach (Winterstein et al., 1993), which is typically based on the hierarchical model used to define the joint distribution, as described in Eq. 1. This method defines the contour in a standard normal U-space, represented by variables $\boldsymbol{u} = \{u_1, u_2, u_3\}$, instead of the original variable space. The Rosenblatt transformation is applied to map the sphere associated with a constant failure probability:

$$u_1 = \Phi^{-1}(F_{H_s}(h)),\ u_2 = \Phi^{-1}(F_{U_w|H_s}(u|h)),\ u_3 = \Phi^{-1}(F_{T_p|H_s,U_w}(t|h,u)) \tag{13}$$

where Φ^{-1} denotes the standard univariate normal Cumulative Distribution Function (CDF), while $F_{H_s}(h)$, $F_{U_w,H_s}(u|h)$ and $F_{T_p,H_s,U_w}(t|h,u)$ correspond to the marginal CDF of H_s, the conditional CDF of U_w given H_s and the conditional CDF of T_p given H_s and U_w, respectively. The failure probability P_f is subsequently determined within the standard normalized U-space:

$$1 - P_f = \int_{G_U(\boldsymbol{u})\leq 0} \Phi(\boldsymbol{u})\, d\boldsymbol{u} \tag{14}$$

where $\Phi(\boldsymbol{u})$ represents the PDF of standard univariate normal distribution. According to the IFORM approach, the failure surface $G_U(\boldsymbol{u})$ is approximated by a convex shape in the transformed space, where the failure boundary is subjected to linearization. In the U-space, events associated with a specified T_R lie on the sphere with radius β_F, known as reliability index, which is computed as:

$$\beta_F = \Phi^{-1}(1 - P_f) \tag{15}$$

The failure probability is then associated to the return period T_R via the average time between two consecutive target events $\Delta\tau$:

$$P_f = \frac{\Delta\tau}{T_R} \tag{16}$$

Based on the reliability index for the prescribed T_R, the sphere is defined in the U-space:

$$\sqrt{u_1^2 + u_2^2 + u_3^2} = \beta_F \tag{17}$$

Finally, to estimate the EC, the transformation from the U-space to the environmental parameter space is performed using the inverse Rosenblatt transformation:

$$h = F_{H_s}^{-1}(\Phi(u_1)),\quad u = F_{U_w|H_s}^{-1}(\Phi(u_2)),\quad t = F_{T_p|H_s,U_w}^{-1}(\Phi(u_3)) \tag{18}$$

In line with the ULS recommendations, EC surfaces corresponding to a return period of 50 years are considered. Subsequently, EC lines are defined from these surfaces based on specific wind turbine conditions that may be critical for the ULS. These conditions are associated with the mean wind speed at the hub height, as schematized in the guidelines' Design Load Cases (DLCs). The mean wind speed considered in the joint distribution is the 1-hour average at a height of 10 meters above sea level $U_{w,1-hr}(10)$. For structural assessment of a FOWT at ULS, the 1-hour mean wind speed at hub height $U_{w,10-min}(z_{hub})$ may be required. In a preliminary design stage, the power law can be applied to estimate the wind speed at any given height z, and a time-averaging correction factor, applicable to the 50-year return period, can be incorporated as specified in IEC 61400-3:

$$U_{w,10-min}(z) = \frac{U_{w,1-hr(z_r)}}{k_1}\left(\frac{z}{z_r}\right)^{\alpha} \tag{19}$$

where z denotes the height and z_r is the reference height above the still water level used for the profile fitting. The time-averaging correction factor k_1 is taken as 0.95. A simulation of the wind field accounting for the roughness and topographic effects would enable a more realistic characterization of the wind speed profile under Mediterranean conditions, including parameters such as the power-law exponent α. However, only a limited number of studies have investigated the value of the power-law exponent for wind speed extrapolation in the MS, and the available works (see, e.g., Farrugia, 2003; Şişman, 2021) are not representative of the specific sites considered in this study. In this work, a power-law exponent of 0.12 was adopted, consistent with the study of Wang and Moan (2024). This value is lower than the widely used 1/7 power law exponent, which is frequently applied to estimate wind speed at the hub height of wind turbines (Peterson and Jr, 1978). The adoption of a lower exponent for offshore locations is also supported by other studies (see, e.g., Hsu et al., 1988; Shu et al., 2016), although the calibration of this parameter should be conducted on a site-specific basis.

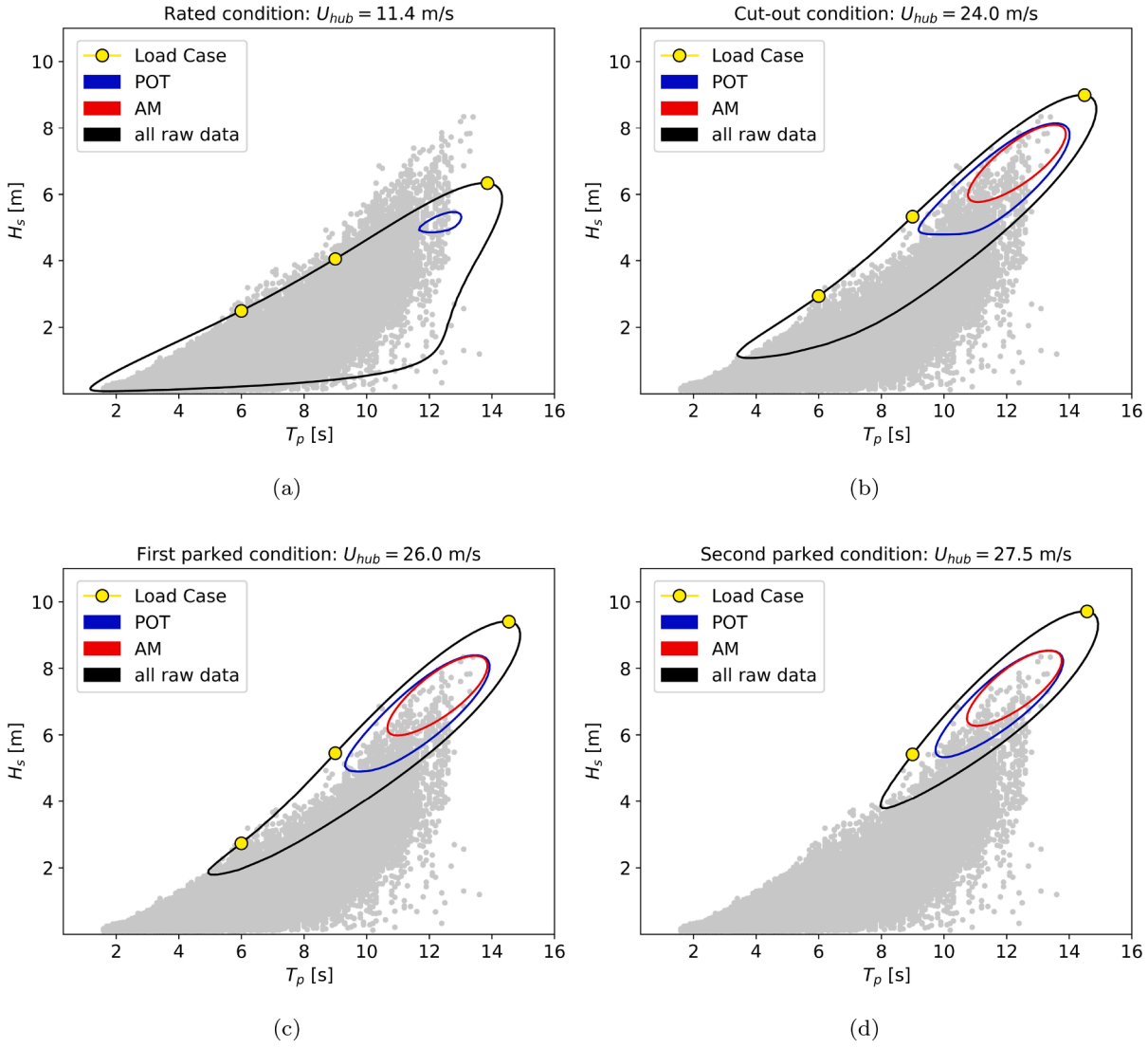

Fig. 8. 50-year $H_s - T_p$ EC lines for POT, AM and the entire dataset under rated, cut-out and parked conditions at site 1 and the selected load cases corresponding to the EC line generated using the entire dataset.

The reference device considered in this study is a semi-submersible FOWT designed to support the DTU 10-MW horizontal-axis wind turbine (Li et al., 2024). The floating platform comprises three pontoons and four columns, with its main geometric characteristics summarized in Table 1. The dynamic characteristics used for load case selection are estimated from the dominant peak positions of the bending moment RAOs, at both an outer column and the central column of the reference system, across different wave directions. These peaks fall in the [5 s; 10 s] wave period range. In addition, the pitch natural period of the reference system, which equals approximately 25 seconds, is taken into account. This value is typical for semi-submersible FOWTs and aligns with observations from other case studies, such as WindFloat (Roddier et al., 2017), OC4-DeepCwind (Coulling et al., 2013; Tran and Kim, 2015), and OUCwind (Bai et al., 2024). However, the presented RAOs and natural frequencies represent general trends; each FOWT, nonetheless, exhibits distinct dynamic characteristics influenced by multiple factors, including the specific site conditions and the broader design context.

Extreme conditions for DLCs 1.6 and 6.1 in DNVGL-ST-0437 (DNVGL-ST-0437, 2016) are selected following the methodology presented by Wang and Moan (2023), suggesting that RAOs for an established floater geometry should be computed under specific conditions.

Table 1
Main dimensions of the semi-submersible platform described in Li et al. (2024).

Parameter	Value
Water depth [m]	50
Draft [m]	22
Column centerline spacing [m]	45
Outer column radius [m]	5.25
Outer column height [m]	26
Central column height [m]	26
Pontoon width [m]	16
Pontoon height [m]	7

The methodology is based on design standards and critical wave periods related to the natural period of motion and the RAOs of internal loads. Wind-sea conditions selected for Site 1 are presented in Table 2, while metocean variables for the remaining sites are provided in Tables A.5-A.6-A.7 of the Appendix A. According to DNVGL-ST-0437 (DNVGL-ST-0437, 2016), a FOWT must be assessed under several operational states, named Design Load Condition (DLC), associated with specific wind conditions, including: power production (DLC 1), power

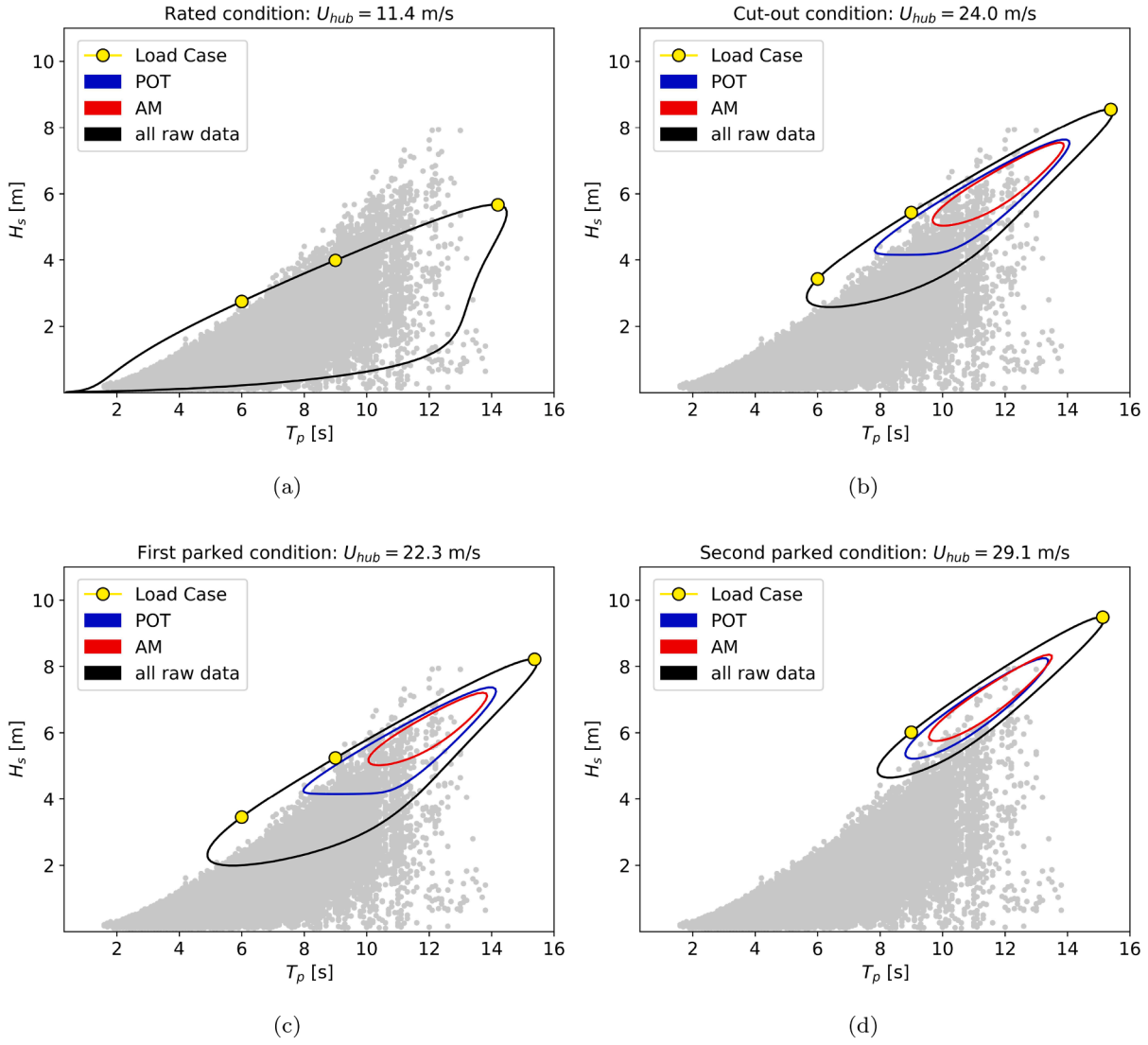

Fig. 9. As in Fig. 8 for site 2.

Table 2
Environmental conditions and load cases for site 1.

Condition	DLC	Load case	U_{hub} [m/s]	U_{1-hr} [m/s]	H_s [m]	T_p [s]
Rated condition	DLC 1.6	LC1	11.40	8.32	2.49	6.00
		LC2	11.40	8.32	4.06	9.00
		LC3	11.40	8.32	6.34	13.86
Cut-out condition	DLC 1.6	LC4	24.00	17.52	2.94	6.00
		LC5	24.00	17.52	5.33	9.00
		LC6	24.00	17.52	8.99	14.49
Parked condition	DLC 6.1	LC7	26.00	18.99	2.73	6.00
		LC8	26.00	18.99	5.45	9.00
		LC9	27.50	20.10	5.41	9.00
		LC10	35.86	26.17	11.12	14.41
		LC11	36.58	26.67	10.78	13.98

production with a fault occurrence (DLC 2), start-up (DLC 3), normal shutdown (DLC 4), emergency stop (DLC 5), parked (DLC 6), parked with a fault occurrence (DLC 7), and transport, installation, maintenance, and repair (DLC 8). Each DLC must be evaluated under different combinations of marine and wind conditions, including, for example, representative wind turbulence models, sea states, wind and wave directionality, sea currents, and water levels. For the purposes of this study, DLCs 1.6 and 6.1 of DNVGL-ST-0437 are selected. These DLCs are stationary and correspond to 50-year extreme sea state conditions, which can be estimated using the EC method. Accordingly, the considered conditions include the rated wind condition (mean wind speed of 11.4 m/s at hub height), the cut-out wind condition (mean wind speed of 25 m/s, with 24 m/s being more critical due to control system behavior), and the parked condition under extreme environmental loading. As schematized in Table 2, LC1 and LC2 are associated with T_p values of 6.0 s and 9.0 s, as these fall within the range (5 s-10 s) where peaks in the RAOs for bending moments are observed. LCs 4-5-7-8 are associated with the same T_p values but different wind conditions (note that such range for T_p is also critical for splitting/praying). Since EC lines shift towards higher peak periods as the wind speed increases, the first and the second parked conditions are selected to include T_p values of 6 s and 9 s, respectively, along the EC lines corresponding to the maximum U_w. LC3 in rated wind conditions is identified with the highest H_s value in the rated condition, while LC10 and LC11 correspond to conditions with the maximum H_s and the maximum U_w on the EC surface. The H_s peak values along the two contour lines for parked conditions are not selected, as they are considered less severe than those corresponding to LC10 and LC11.

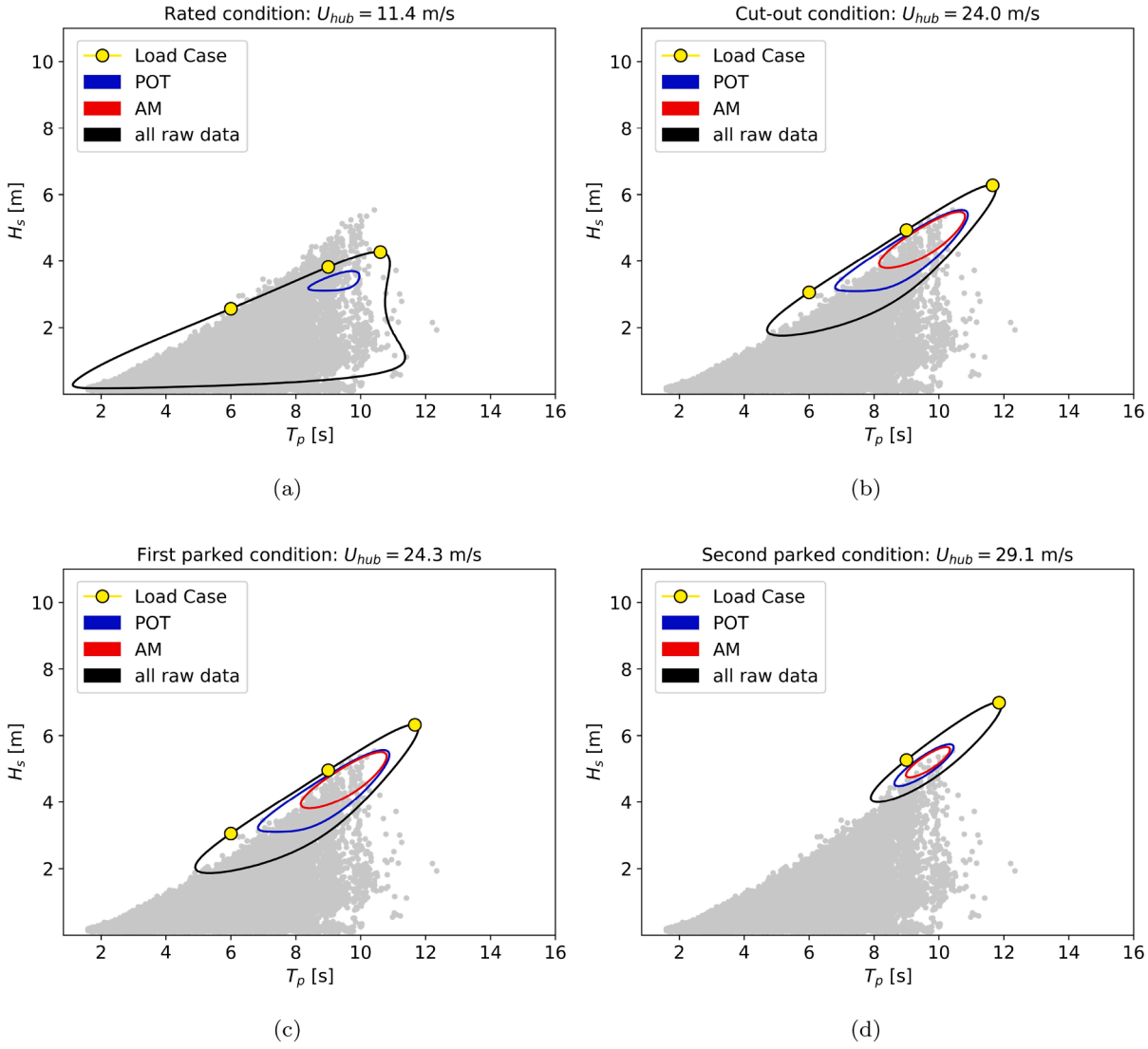

Fig. 10. As in Fig. 8 for site 3.

3. Data

This study relies on the long-term hindcast data provided by the Department of Civil, Chemical, and Environmental Engineering of the University of Genoa (Lira-Loarca et al., 2022). The hindcast covers the whole MS, with variable resolution from approximately 25 km off-shore to approximately 300 m at the coast. At each node, hourly time series of H_s, T_p and U_w are retained, covering a timeframe of 42 years (from 1979 to 2020). Four locations with water depths ranging between 50 and 100 m are selected to consider sites associated with varying potentials ****[see Table 3 and Fig. 1](Ferrari et al., 2020; Martinez and Iglesias, 2021). Data from a North Sea location are employed to compare metocean conditions with a Mediterranean site, both suitable for the installation of semi-submersible FOWTs (Messmer et al., 2023). For the North Sea site, the ERA5 reanalysis dataset produced by ECMWF is used (Hersbach et al., 2020), spanning the same timeframe as the dataset adopted for the MS.

Table 3
Coordinates of the target sites (RS: WGS84).

site ID	lon	lat	basin
1	8.1100	40.2600	West Thyrrenean
2	12.0540	37.6500	South Thyrrenean
3	18.1660	40.8000	Adriatic
4	3.9047	42.9600	Gulf of Lion
5	4.2748	60.6516	North Sea

4. Results & discussion

We first present the results for the uni-variate extreme value distributions used to describe H_s; for the sake of clarity, reference is made to site 1 only. In all cases, the 95% Confidence Interval (CI) of the T_R estimates embed the vast majority of empirical data, demonstrating the reliability of the distributions, as further demonstrated by the QQplot (Wilk and Gnanadesikan, 1968) (Fig. 2, panels a,b for POT data; panels c,d for AM data; panels e,f for total data). However, while either AM and POT data yield comparable values for higher return periods, the exponentiated Weibull distribution tends to overpredict values for return periods exceeding 1 year. This overestimation persists despite utilizing the least squares fitting method and affects the subsequent characterization of extreme wind-wave conditions. The overestimation resulting from the use of the complete dataset, as compared to employing only

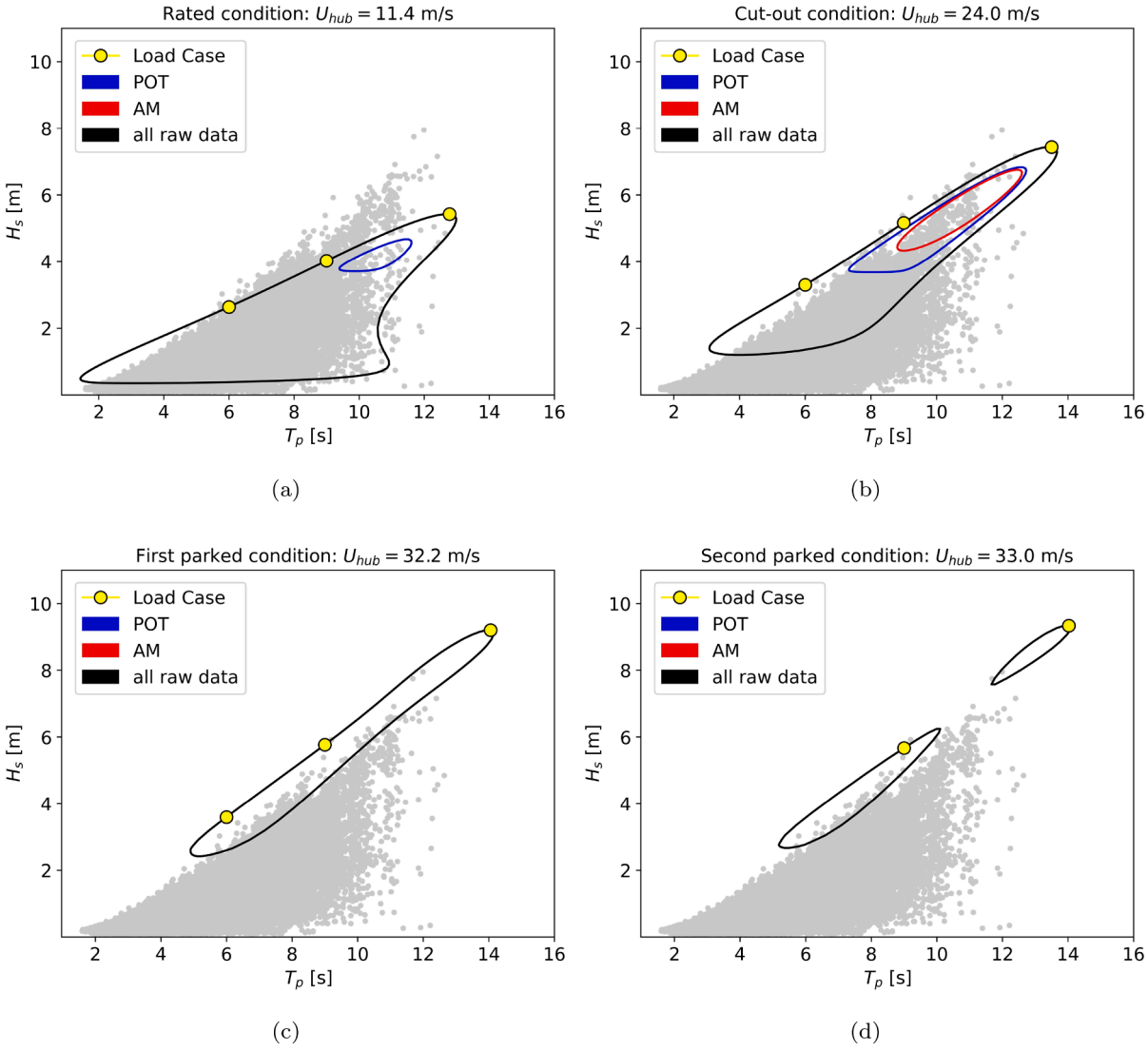

Fig. 11. As in Fig. 8 for site 4.

storm maxima, has also been reported by Coe et al. (2022) and affects the shape of the ECs.

The conditional distribution of U_w is analyzed across different H_s classes to estimate the shape and scale parameters. Fig. 3 provides examples of the conditional distribution of U_w for two H_s classes. For higher H_s (between 5.5 m and 6 m), the conditional distribution of U_w exhibits improved alignment. Indeed, data deviating from the Weibull distribution for the lower H_s classes are mainly associated with values of U_w near zero, which are absent in the upper H_s classes. The scale parameter of the Weibull distribution shows a remarkable fit (Fig. 4b) across the H_s classes, while higher values of H_s yield noisy estimates of the shape parameter (see Eq. 4 and Fig. 4a).

For the conditional lognormal distribution of T_p given U_w and H_s, the latter plays the major role. This is evident in Fig. 5, which shows the empirical values of the mean $T_p(h,u)$, also denoted as $\bar{t}(u,h)$, (see Fig. 5a and Eq. 10) and the empirical COV of T_p (Fig. 5b). The first parameter is used to evaluate $\theta(h)$, and subsequently $\mu_{T_p}(h,u)$ while the second is the ratio between the empirical standard deviation and mean of $T_P(h,u)$, which together are used to assess the coefficients of $\nu_{T_p}(h,u)$. The parameters $\mu_{T_p}(h,u)$ and $\nu_{T_p}(h,u)$ are then employed to estimate the parameters of the lognormal distribution, namely $\mu_{\ln(T_p)}(h,u)$ and $\sigma^2_{\ln(T_p)}(h,u)$ (see Eq. 6). As expected, T_p increases according to H_s, while the opposite trend (although with lower magnitude) is found with respect to U_w, as shown by the behavior of θ (which expresses the ratio between the normalized T_p and the normalized U_w; see Eq. 10 and Fig. 6 (a)). Overall, the model exhibits higher deviations for lower H_s and U_w values, as shown by the residual matrix of the mean T_p (Fig. 6 (b)). Conversely, the residuals diminish under extreme conditions, suggesting improved model accuracy for more energetic states. The parameters of the distributions for all sites are summarized in Table 4.

Load cases corresponding to rated, cut-out, first parked, and second parked wind conditions are then selected along the EC lines obtained from the EC surfaces illustrated in the Figs. A.13-A.14-A.15-A.16 of the Appendix A. The EC lines are evaluated for each wind condition using the AM, POT, and the entire H_s dataset. Initially, the results obtained using AM, POT, and all raw data are compared through the EC lines displayed in the Figs. 8-9-10-11. The analysis reveals that resonance conditions for pitch motion, associated with the lowest natural frequency among a semi-submersible floater's six motions, cannot occur across the four sites. In fact, the typical natural frequency for pitch motion in semi-submersible floaters is approximately 25 s, far off from the wave periods associated with a 50-year return period at the selected sites. As a matter of fact, the Mediterranean wave climate is characterized by shorter

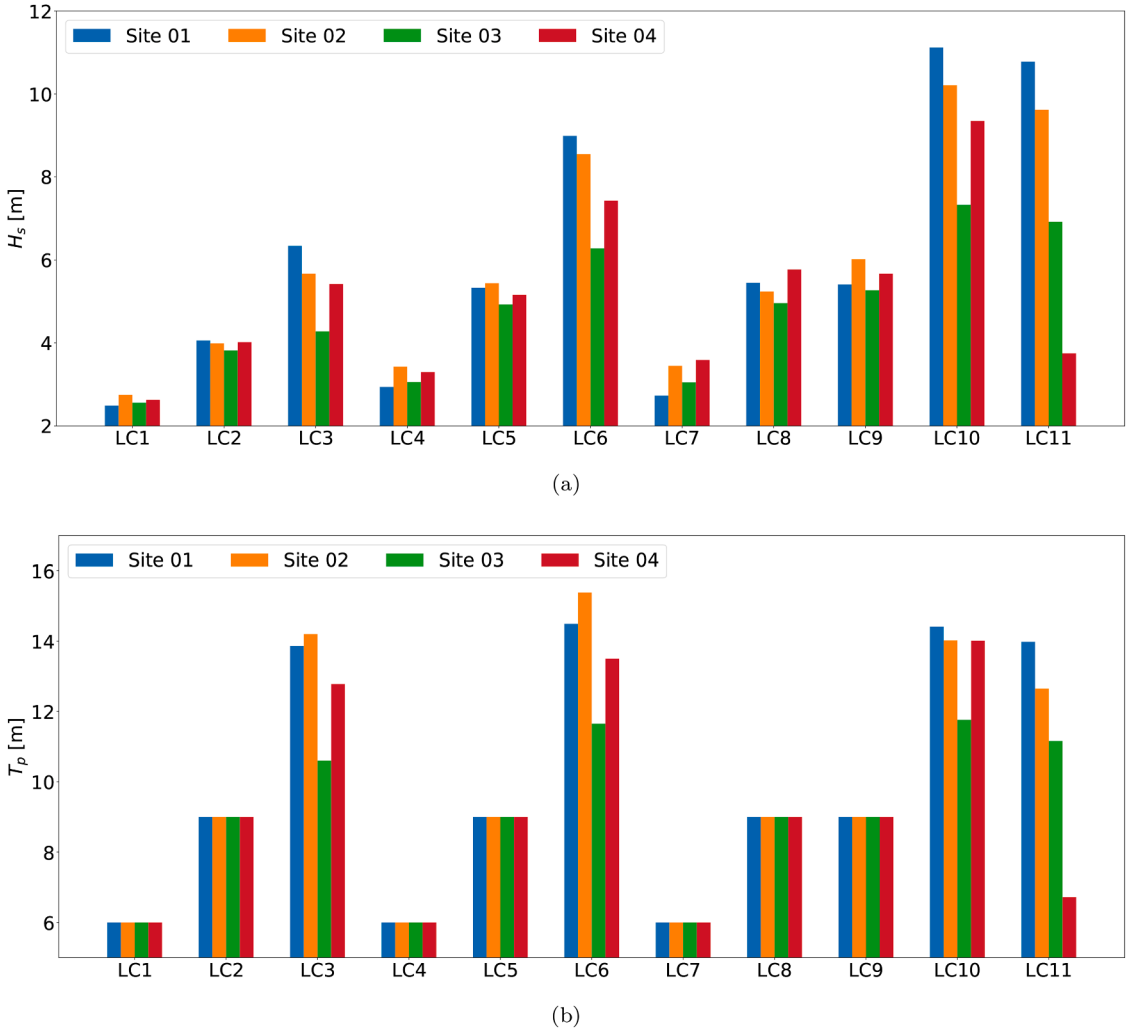

Fig. 12. (a) H_s and (b) T_p values across the four sites under load cases LC1-LC11.

waves than those observed in the Northern Europe. Fig. 7 supports this evidence by comparing the relationship between H_s and T_p at Site 1 in the MS and a location in the North Sea, both considered suitable for the installation of semi-submersible FOWTs. The North Sea site exhibits extreme events with longer T_p, which may approach the pitch natural frequency of FOWTs. This has implications for the design process, even in its early stages. A commonly accepted preliminary design criterion requires pitch and roll natural periods to exceed 25 s to avoid resonance in rigid-body motion, a feature based on typical Northern European metocean conditions (Li et al., 2024). This constraint influences the structural geometry, particularly the submerged components, as added mass plays a key role in determining natural frequencies. Consequently, satisfying stricter criteria may necessitate larger and heavier structures to achieve greater mass and added mass, thereby increasing the natural periods. Moreover, the core of the joint H_s-T_p distribution in the North Sea is shifted toward longer and higher waves compared to the MS, which may also affect fatigue assessment.

The discussion then focuses on the selected load cases derived exclusively from the EC lines estimated using the full dataset. As expected, the extreme values predicted by the EC corresponding to the complete dataset are overestimated across all four sites, particularly for higher H_s and T_p. This is obviously due to the marginal distribution of H_s (see Fig. 2e, f), as it is the only component that differs in the assessment of the joint distribution, and yields higher values than the GEV and GPD for long return periods. On the other hand, the latter exhibit closer alignments, consistent to the respective H_s/T_p curves (Fig. 2a, b and c, d). Across the four sites, the EC surfaces can be sliced in correspondence of the rated condition for the POT and the entire data set, except at site 2, where wind-sea combinations corresponding to the AM and POT EC surfaces are predicted under higher wind conditions, but the rated. The other target wind conditions intersect the EC surfaces estimated with POT, AM, and the entire dataset. In these instances, the EC lines of AM are enclosed within those obtained through POT data. The differences in their H_s predictions diminish under high wind conditions. Under the second parked condition, at site 2, the H_s prediction corresponding to higher T_p values exceeds that of the EC line of AM; however, their difference remains negligible for load case selection purposes. At sites 1 and 3, the wind speeds to include T_p values of 6 s under the first parked condition and 9 s under the second parked condition along the EC lines range between 24.3 m/s and 29.1 m/s. At Site 1, the wind speed associated with Tp equal to 6 s and 9 s (for the first and second parked conditions, respectively) results in a narrower interval embedded within the above limits. This increase is comparatively lower than in observed locations in the North Sea or the Atlantic Ocean, where the difference between the U_w in the second park and the cut-out conditions can reach up to 70% (Wang and Moan, 2023). The wind speed associated with the second parked condition is equivalent for sites 2 and 3. The EC surfaces at higher U_w for these two sites exhibit narrow EC lines, indicating limited variability in terms of H_s and T_p, particularly at higher sea state parameters. In contrast, site 1, located in Sardinia, displays a rounder EC

Table 4
Parameters for the marginal PDF of H_s, $f_{H_s}(h)$, with the AM, POT and all raw data, for the conditional PDF of U_w given H_s, $f_{U_w|H_s}(u|h)$, and for the conditional PDF of T_p given H_s and U_w, $f_{T_p|H_s,U_w}(t|h,u)$.

Probability	Parameter	Equation	Site 1	Site 2	Site 3	Site 4
$f_{H_s}(h)$ AM	μ	GEV	6.90	5.96	4.44	5.31
	σ	GEV	0.72	0.68	0.47	0.71
	ξ	GEV	0.26	0.02	0.21	0.04
$f_{H_s}(h)$ POT	μ	GP	4.78	4.15	3.07	3.67
	σ	GP	1.34	1.08	0.80	0.92
	ξ	GP	-0.28	-0.15	-0.22	-0.07
$f_{H_s}(h)$	k	Eq. 2	1.17	1.04	1.07	1.01
	α	Eq. 2	1.10	1.91	1.69	2.35
	λ	Eq. 2	1.23	0.83	0.66	0.70
$f_{H_s\|U_w}(h\|u)$	a_1	Eq. 4	2.12	2.62	2.33	4.29
	a_2	Eq. 4	1.69	0.98	1.24	0.01
	a_3	Eq. 4	0.37	0.72	1.28	3.68
	b_1	Eq. 4	2.07	1.04	0.72	-5.14
	b_2	Eq. 4	4.09	5.88	6.92	13.95
	b_3	Eq. 4	0.74	0.63	0.62	0.34
$f_{T_p\|H_s,U_w}(t\|h,u)$	m_1	Eq. 11	-0.00	-0.00	-0.01	-0.01
	m_2	Eq. 11	-0.29	-0.50	-0.21	-0.35
	γ	Eq. 8	1.00	1.00	1.00	1.00
	e_1	Eq. 9	0.34	2.76	2.74	3.04
	e_2	Eq. 9	6.03	3.14	2.67	2.06
	e_3	Eq. 9	0.34	0.55	0.60	0.74
	f_1	Eq. 9	1.90	0.87	0.78	-3.01
	f_2	Eq. 9	3.55	5.38	6.14	10.93
	f_3	Eq. 9	0.79	0.66	0.67	0.40
	k_1	Eq. 12	0.03	0.02	0.02	0.03
	k_2	Eq. 12	0.26	0.23	0.31	0.30
	k_3	Eq. 12	-0.68	-0.39	-0.69	-0.75

surface profile for higher sea state parameters, resulting in sea state combinations distributed over a wider range of values. For site 2, the first parked condition cannot occur as the U_w value, equivalent to 22.3 m/s, falls below the cut-out threshold. Specifically, under cut-out conditions, the T_p value equivalent to 6 s is already close to the minimum values of the EC line. Finally, site 4 is characterized by the most severe parked conditions in terms of wind speeds, which exceed 32 m/s. Specifically, the methodology used to define the load cases in the parked conditions cannot be strictly applied to this site due to the resulting concave shape of the EC surface, which features two U_w peaks above the first parked condition. In this case, the second parked condition is determined by including the T_p of 9 s at the boundary with the highest T_p values from one of the two EC lines.

Figs. 12(a)(b) illustrate the loading conditions for the four sites in terms of H_s and T_p. Notably, the variability is limited across sites 1 and 2 (in Sardinia and Sicily) for all load cases. Although site 4 exhibits higher U_w under parked conditions, the corresponding wind speeds in LC10-LC11 (33.2 m/s and 34.64 m/s) are not the highest across the four sites; under these conditions, Site 1 exhibits higher H_s values and the longest sea states in terms of T_p. Site 2 is characterized by the longest T_p values under the rated and cut-out conditions, exhibiting the maximum T_p value among all the load cases. For combinations where T_p equals 6 s and 9 s, none of the sites distinctly dominate in terms of H_s. Finally, the minimum loading with the selected wind-sea parameters would be applied to a FOWT at site 3 in the Adriatic Sea. For nearly all load cases, sites 1 and 2 exhibit the highest loading in terms of H_s and the longest sea states. These observations are based on the loading level associated with specific wind-sea parameter combinations selected using the preliminary methodology. However, assessing the suitability of a particular site for the installation of a semi-submersible FOWT should integrate these considerations with the estimation of additional parameters, such as the Annual Energy Production (AEP) linked to the local wind resource. Furthermore, the RAOs for a defined geometry should be evaluated to enable a more accurate selection of load cases.

5. Conclusions

The exploitation of wind energy in the Mediterranean Sea (MS) is garnering increasing attention within the offshore renewable energy sector, with semi-submersible floating technology identified as the most promising in this context. However, existing design criteria and recommendations for Floating Offshore Wind Turbine (FOWT) structures are mainly tailored to North Sea and Atlantic Ocean climates, with limited focus on the Mediterranean basin. On this note, in this research we evaluate the DNV and IEC guidelines for the ULS to compute the loading condition for FOWT at four sites spread in the MS. We generate EC surfaces using the IFORM for a 50-year return period, taking advantage of hindcast data (U_w, H_s and T_p) defined in the 1979-2020 period. The combinations of wave parameters are represented as EC lines, with design states selected to align with target wind speeds as specified in the DLCs guidelines. The selection of target design loads in the MS provides insights into the combined wind-sea excitations required to perform an extreme response analysis of a FOWT. Moreover, it serves as a useful basis for investigating how uncertainties in data extraction propagate within the 3D IFORM framework under Mediterranean conditions.

The results are presented for each site under four wind conditions, with EC lines evaluated for three EC surfaces established by differently selecting the initial data set, that is AM, POT method, and the entire time series. Load cases are selected from the EC line obtained using the full dataset, following a methodology proposed by Wang and Moan (2023). The dynamic characteristics of reference FOWTs established for Northern European environmental conditions are incorporated into this approach, due to the lack of systems tailored explicitly for the MS.

Our findings indicate that resonance associated with the natural frequency of pitch motion is unlikely to occur under Mediterranean climates, as typical sea states are associated to wave periods below 20 s. Unlike in the MS, extreme metocean conditions in the North Sea can approach the natural pitch frequencies of semi-submersible FOWTs. This distinction may significantly influence floater design from the early stages, potentially resulting in lighter configurations in the Mediterranean, as preliminary criteria on natural frequencies are primarily based on the Northern European climate. Results also reveal that the highest H_s values on the EC lines are predominantly influenced by the choice of marginal distribution: the exponentiated Weibull distribution, usually employed for modeling the entire data sets, tends to overestimate H_s values at high return periods, and this is reflecting to the resulting EC lines.

The two sites located in the south-west Thyrrenean Sea yield aligned environmental contours, and this is reflecting on similar load cases, being overall characterized by the highest combined wind-sea parameters. By contrast, the location in the Adriatic Sea is characterized by the lowest combined H_s and T_p parameters, with the exception of a few load cases. However, variations in wind-sea parameters are not always directly associated with the response effects on the structure on purpose. To more accurately identify the points on the EC surface that may maximize specific response effects, the complete RAO functions, rather than just their first peaks, should be evaluated for the specific geometry of the FOWT. This approach would provide a clearer understanding of the relationship between environmental conditions and structural responses.

The work-flow and design environmental stressors presented in this study provide a preliminary tool to compare potential locations for FOWT installations in the MS, based on the predicted conditions expected to result in the highest excitation under ULS. This can aid in tailoring future designs specifically for the Mediterranean region, helping to avoid overly conservative estimations and scantling. Indeed, site-

specific analyses are essential for achieving lighter, more efficient, and cost-effective platform designs–particularly in the Mediterranean Sea, where wind speeds are milder and wave conditions are generally characterized by lower heights and shorter periods than those observed in Northern European seas. In this context, adopting a refined probabilistic approach that accounts for the statistical dependence between key environmental variables (e.g., H_s, T_p, U_w) allows for more precise and efficient FOWT design calibration. In contrast, simplified approaches based on safety factors or assumptions, as in IEC 61400-3, where the dependency of T_p on H_s and U_w is neglected – may lead in overly conservative estimations. In the end, such approach is set within the context of reducing the costs associated to these developments, which is crucial for the large-scale deployment of FOWT technology, thereby supporting its broader adoption in the renewable energy sector in the MS.

Data availability statement

In the context of the Mediterranean Sea, the hindcast has been used for several scientific publications (https://meteocean.science/research/publications) and for different coastal and ocean engineering applications in the framework of knowledge transfer with the industry (https://meteocean.science/#partnerships). The nodes where data are available can be visualized at: https://forecast.meteocean.science/hindcast/. The ERA5 data used are freely available through the C3S Climate Data Store (https://cds.climate.copernicus.eu) and the ECMWF archive (https://www.ecmwf.int/en/forecasts/datasets/archive-datasets).

All the scripts were developed in a Python 3.12 environment and take advantage of the following libraries: below: Numpy, Pandas, Scipy, Matplotlib, Virocon and Statsmodels.

CRediT authorship contribution statement

Elisa Marchelli: Writing – original draft, Visualization, Software, Methodology, Investigation, Formal analysis, Conceptualization; **Francesco De Leo:** Writing – review & editing, Supervision, Software, Methodology, Conceptualization; **Giovanni Besio:** Writing – review & editing, Supervision, Data curation, Conceptualization; **Cesare Mario Rizzo:** Writing – review & editing, Validation, Supervision, Conceptualization.

Declaration of competing interest

The authors declare that they have no known competing financial interests or personal relationships that could have appeared to influence the work reported in this paper.

Appendix A. Additional Results, Figures, and Tables

Table A.5
Environmental conditions and load cases for site 2.

Condition	DLC	Load case	U_{hub} [m/s]	U_{1-hr} [m/s]	H_s [m]	T_p [s]
Rated condition	DLC 1.6	LC1	11.40	8.32	2.75	6.00
		LC2	11.40	8.32	3.99	9.00
		LC3	11.40	8.32	5.67	14.20
Cut-out condition	DLC 1.6	LC4	24.00	17.52	3.43	6.00
		LC5	24.00	17.52	5.44	9.00
		LC6	24.00	17.52	8.55	15.38
Parked condition	DLC 6.1	LC7	22.30	16.30	3.45	6.00
		LC8	22.30	16.39	5.24	9.00
		LC9	29.10	21.24	6.02	9.00
		LC10	35.27	25.72	10.21	14.02
		LC11	36.93	26.93	10.48	12.65

Table A.6
Environmental conditions and load cases for site 3.

Condition	DLC	Load case	U_{hub} [m/s]	U_{1-hr} [m/s]	H_s [m]	T_p [s]
Rated condition	DLC 1.6	LC1	11.40	8.32	2.56	6.00
		LC2	11.40	8.32	3.82	9.00
		LC3	11.40	8.32	4.28	10.06
Cut-out condition	DLC 1.6	LC4	24.00	17.52	3.06	6.00
		LC5	24.00	17.52	4.93	9.00
		LC6	24.00	17.52	6.28	11.65
Parked condition	DLC 6.1	LC7	24.30	17.73	3.05	6.00
		LC8	24.30	17.73	4.96	9.00
		LC9	29.10	21.25	5.27	9.00
		LC10	35.27	24.01	7.33	11.76
		LC11	36.93	24.81	6.92	11.16

Table A.7
Environmental conditions and load cases for site 4.

Condition	DLC	Load case	U_{hub} [m/s]	U_{1-hr} [m/s]	H_s [m]	T_p [s]
Rated condition	DLC 1.6	LC1	11.40	8.32	2.63	6.00
		LC2	11.40	8.32	4.02	9.00
		LC3	11.40	8.32	5.42	12.78
Cut-out condition	DLC 1.6	LC4	24.00	17.52	3.30	6.00
		LC5	24.00	17.52	5.16	9.00
		LC6	24.00	17.52	7.43	13.50
Parked condition	DLC 6.1	LC7	32.20	18.61	3.59	6.00
		LC8	32.20	18.61	5.77	9.00
		LC9	33.00	24.10	5.67	9.00
		LC10	35.27	25.74	9.35	14.01
		LC11	36.93	26.95	3.75	6.72

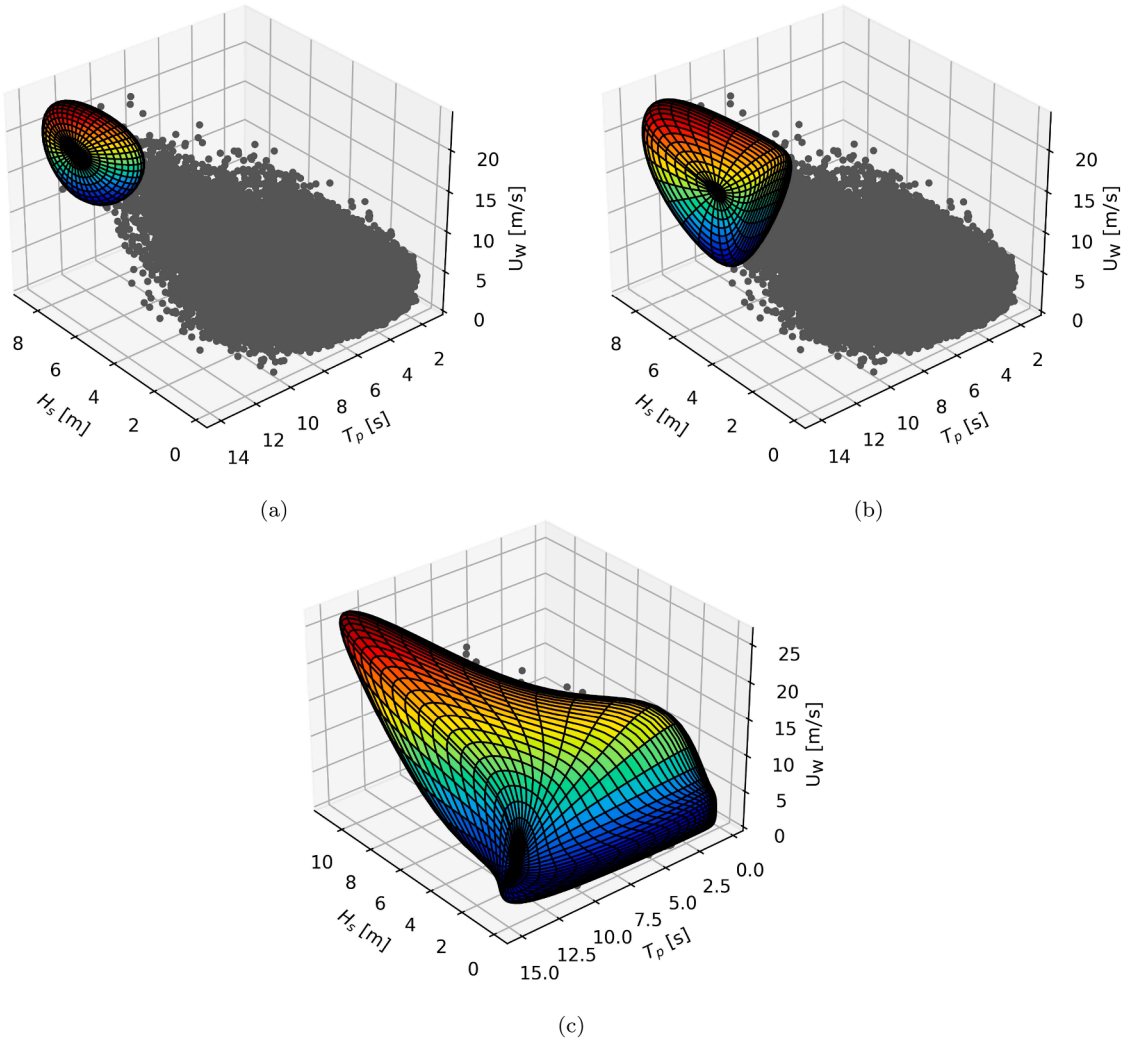

Fig. A.13. 50-year $H_s - T_p - U_w$ EC surface of site 1 for the AM, the POT and the entire dataset.

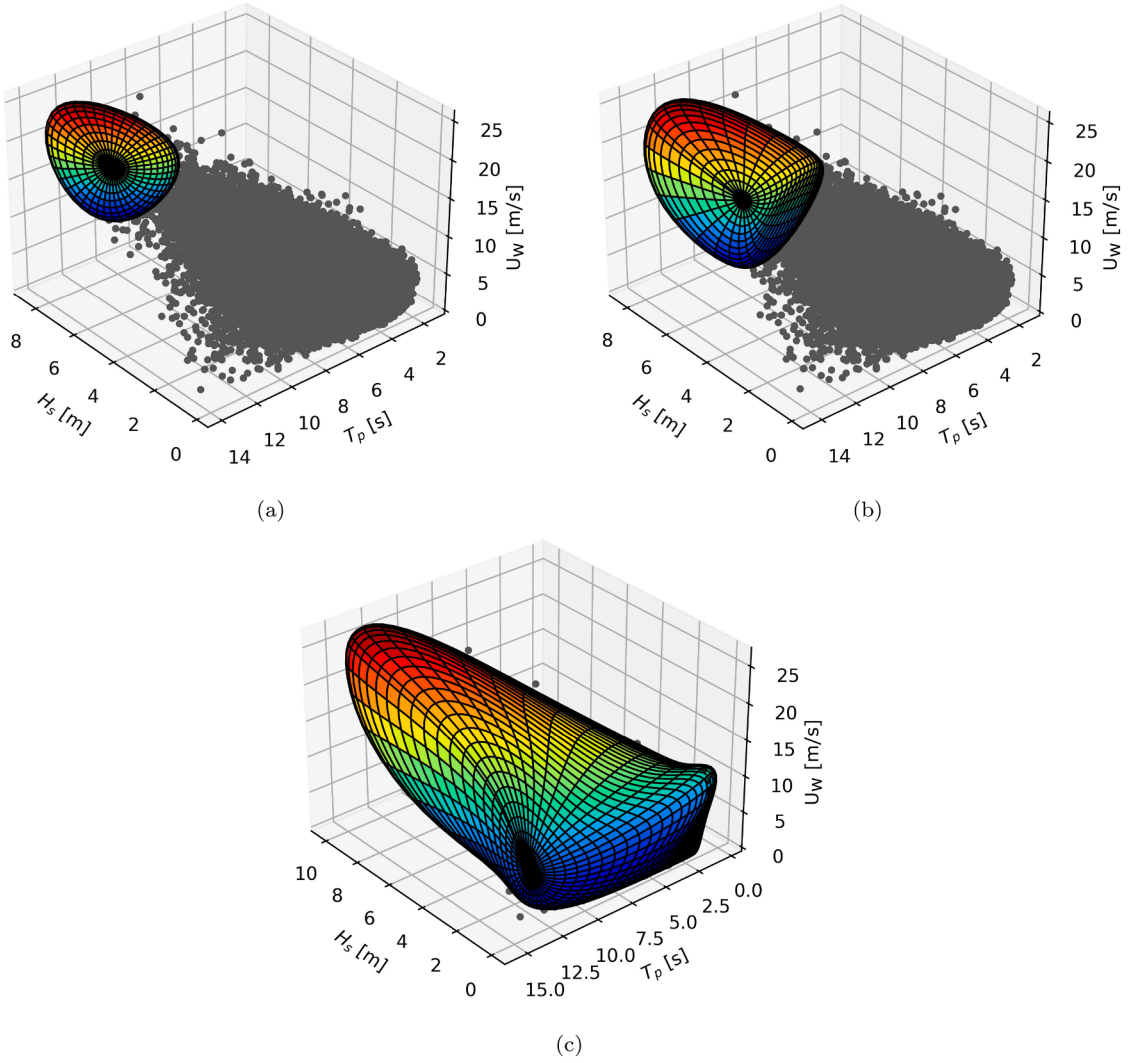

Fig. A.14. As in Fig. A.13 for site 2.

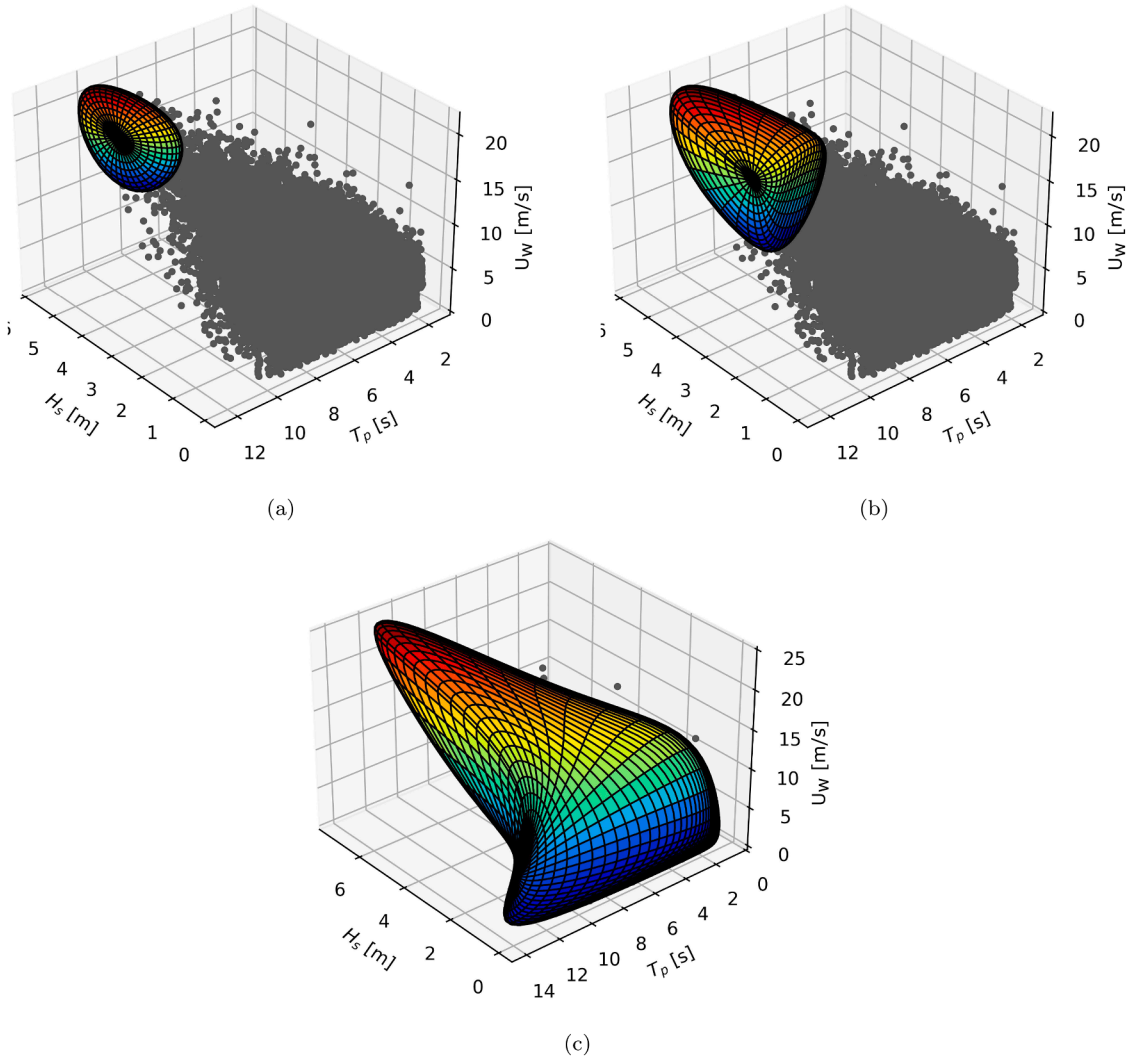

Fig. A.15. As in Fig. A.13 for site 3.

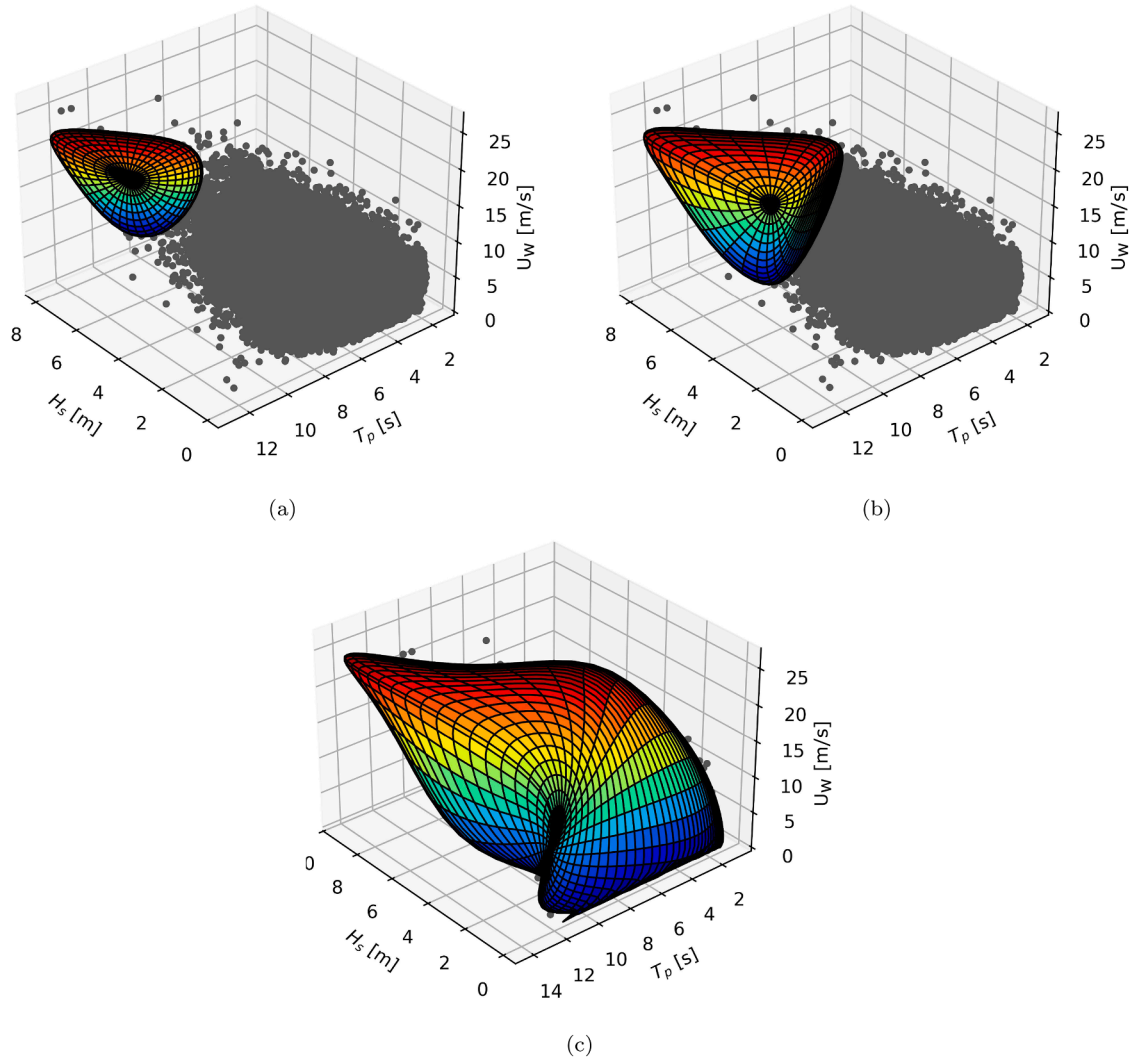

Fig. A.16. As in Fig. A.13 for site 4.

References

Bai, H., Xu, K., Zhang, M., Yuan, W., Jin, R., Li, W., Gao, S., Li, H., 2024. Theoretical and experimental study of the high-frequency nonlinear dynamic response of a 10 mw semi-submersible floating offshore wind turbine. Renew. Energy 231, 120952. https://doi.org/10.1016/j.renene.2024.120952. https://doi.org/10.1016/j.renene.2024.120952

Barbariol, F., Davison, S., Falcieri, F.M., Ferretti, R., Ricchi, A., Sclavo, M., Benetazzo, A., 2021. Wind waves in the mediterranean sea: an era5 reanalysis wind-based climatology. Front. Marine Sci. 8, 760614.

Bezak, M. B.N., Šraj, M., 2014. Comparison between the peaks-over-threshold method and the annual maximum method for flood frequency analysis. Hydrol. Sci. J. 59, 959–977. https://doi.org/10.1080/02626667.2013.831174

Chirosca, A.M., Rusu, L., 2022. Characteristics of the wind and wave climate along the european seas focusing on the main maritime routes. J. Marine Sci. Eng. 10, 75.

Coe, R.G., Manuel, L., Haselsteiner, A.F., 2022. On limiting the influence of serial correlation in metocean data for prediction of extreme return levels and environmental contours. Ocean Eng. 266, 113032. https://doi.org/10.1016/j.oceaneng.2022.113032

Coles, S., Bawa, J., Trenner, L., Dorazio, P., 2001. An introduction to statistical modeling of extreme values. Vol. 208. Springer.

Coulling, A., Goupee, A., Robertson, A., Jonkman, J., Dagher, H., 2013. Validation of a fast semi-submersible floating wind turbine numerical model with deepcwind test data. J. Renew. Sustain. Energy 5. https://doi.org/10.1063/1.4796197

DNVGL-ST-0437 , 2016. Standard dnv gl st 0437: Loads and site conditions for wind turbines. DNV GL: Oslo. Number DNVGL-ST-0437 In Norway.

Farrugia, R.N., 2003. The wind shear exponent in a mediterranean island climate. Renew. Energy 28, 647–653.

Ferrari, F., Besio, G., Cassola, F., Mazzino, A., 2020. Optimized wind and wave energy resource assessment and offshore exploitability in the mediterranean sea. Energy 190, 116447.

Ferreira, J.A., Soares, C.G., 1998. An application of the peaks over threshold method to predict extremes of significant wave height. J. Offshore Mech. Arctic Eng. 120, 165–176. https://doi.org/10.1115/1.2829537

Goda, Y., 2000. Random seas and design of maritime structures. Adv. Series Ocean Engin. 33. https://doi.org/10.1142/3587

Haselsteiner, A.F., Ohlendorf, J.H., Wosniok, W., Thoben, K.D., 2017. Deriving environmental contours from highest density regions. Coastal Eng. 123, 42–51.

Haselsteiner, A.F., Sander, A., Ohlendorf, J.H., Thoben, K.D., 2020. Global hierarchical models for wind and wave contours: Physical interpretations of the dependence functions. In: International Conference on Offshore Mechanics and Arctic Engineering. American Society of Mechanical Engineers. P. V02AT02A047.

Haselsteiner, A.F., Thoben, K.D., 2020. Predicting wave heights for marine design by prioritizing extreme events in a global model. Renew. Energy 156, 1146–1157. https://doi.org/10.1016/j.renene.2020.04.112

Hauteclocque, G.D., Mackay, E., Vanem, E., 2022. Quantitative comparison of environmental contour approaches. Ocean Eng. 245. https://doi.org/10.1016/j.oceaneng.2021.110374. https://doi.org/10.1016/j.oceaneng.2021.110374

Hersbach, H., Bell, B., Berrisford, P., Hirahara, S., Horányi, A., noz Sabater, J.M., Nicolas, J., Peubey, C., Radu, R., Schepers, D., Simmons, A., Soci, C., Abdalla, S., Abellan, X., Balsamo, G., Bechtold, P., Biavati, G., Bidlot, J., Bonavita, M., Thépaut, J.N., 2020. The era5 global reanalysis. Quarterly Journal of the Royal Meteorological Society 146. https://doi.org/10.1002/qj.3803

Hsu, S., Meindl, E.A., Gilhousen, D.B., 1988. Determining the power-law wind-profile exponent under near-neutral stability conditions at sea. pp. 757–765.

Huseby, A.B., Vanem, E., Natvig, B., 2015. Alternative environmental contours for structural reliability analysis. Structural Safety 54, 32–45. https://doi.org/10.1016/j.strusafe.2014.12.003

Johannessen, K., Meling, T.S., Haver, S.K., 2002. Joint distribution for wind and waves in the northern north sea. International Journal of Offshore and Polar Engineering 12.

Lang, M., Ouarda, T.B., Bobée, B., 1999. Towards operational guidelines for over-threshold modeling. Journal of hydrology 225, 103–117.
Leo, F.D., Besio, G., Briganti, R., Vanem, E., 2021. Non-stationary extreme value analysis of sea states based on linear trends. analysis of annual maxima series of significant wave height and peak period in the mediterranean sea. Coastal Eng. 167, 103896. https://doi.org/10.1016/j.coastaleng.2021.103896
Li, W., Wang, S., Moan, T., Gao, Z., Gao, S., 2024. Global design methodology for semi-submersible hulls of floating wind turbines. Renew. Energy 225, 120291. https://doi.org/10.1016/j.renene.2024.120291
Li, X., Zhang, W., 2020. Long-term assessment of a floating offshore wind turbine under environmental conditions with multivariate dependence structures. Renew. Energy 147, 764–775. https://doi.org/10.1016/j.renene.2019.09.076
Lira-Loarca, A., Cáceres-Euse, A., De-Leo, F., Besio, G., 2022. Wave modeling with unstructured mesh for hindcast, forecast and wave hazard applications in the mediterranean sea. Appl. Ocean Res. 122.
Met Office , 2010. Cartopy: a cartographic python library with a matplotlib interface. Exeter, Devon. https://scitools.org.uk/cartopy.
Martinez, A., Iglesias, G., 2021. Multi-parameter analysis and mapping of the levelised cost of energy from floating offshore wind in the mediterranean sea. Energy Convers. Manag. 243.
Messmer, T., Ran, X., Benifla, V., Lutz, M., Adam, F., Bachynski-Polić, E.E., Hölling, M., 2023. Overview of the potential of floating wind in europe based on met-ocean data derived from the era5-dataset. IOP Publishing, p. 12021.
Mikulić, A., Parunov, J., 2023. Environmental contours in the adriatic sea for design and analysis of marine structures. J. Marine Sci. Eng. 11, 899.
Morgan, E., Lackner, M., Baise, L., 2011. Probability distribution for offshore wind speeds. Energy Conver. Manag. 52, 15–26. https://doi.org/10.1016/j.enconman.2010.06.015
Luceño, A.L., Menendez, M., Mendez, F., 2006. The effect of temporal dependence on the estimation of the frequency of extreme ocean climate events. Proc. Royal Society A: Mathem., Phys. Eng. Sci. 462, 1683–1697. https://doi.org/10.1098/rspa.2005.1652
Peterson, E.W., Jr, J. P.H., 1978. On the use of power laws for estimates of wind power potential. J. Appl. Meteorol. Climatol. 17, 390–394.
Pfanzagl, J., 1994. Parametric Statistical Theory. De Gruyter, Berlin, New York. https://doi.org/10.1515/9783110889765
Roddier, D., Cermelli, C., Aubault, A., Peiffer, A., 2017. Summary and conclusions of the full life-cycle of the windfloat fowt prototype project. https://doi.org/10.1115/OMAE2017-62561
Şişman, E., 2021. Power law characteristics of trend analysis in turkey. Theor. Appl. Climatol. 143, 1529–1541.
Shu, Z., Li, Q., He, Y., Chan, P., 2016. Observations of offshore wind characteristics by doppler-lidar for wind energy applications. Appl. Energy 169, 150–163.
Silva-González, F., Heredia-Zavoni, E., Montes-Iturrizaga, R., 2013. Development of environmental contours using nataf distribution model. Ocean Eng. 58, 27–34. https://doi.org/10.1016/j.oceaneng.2012.08.008
Soares, C., 1993. Long term distribution of non-linear wave induced vertical bending moments. Marine Struc. 6, 475–483. https://doi.org/10.1016/0951-8339(93)90033-Y
Soukissian, T., Kalantzi, G., Karagali, I., 2006. De-clustering of hs-time series for applying the peaks-over-threshold method.
Teena, N., Kumar, V.S., Sudheesh, K., Sajeev, R., 2012. Statistical analysis on extreme wave height. Nat. Hazards 64, 223–236.
Tran, T.T., Kim, D.H., 2015. The coupled dynamic response computation for a semi-submersible platform of floating offshore wind turbine. J. Wind Eng. Ind. Aerodyn. 147, 104–119. https://doi.org/10.1016/j.jweia.2015.09.016
Vanem, E., 2015. Uncertainties in extreme value modelling of wave data in a climate change perspective. J. Ocean Eng. Marine Energy 1, 339–359.
Vanem, E., Bitner-Gregersen, E.M., 2015. Alternative environmental contours for marine structural design-a comparison study. J. Offshore Mech. Arctic Eng. 137, 51601.
Velarde, J., Vanem, E., ft, C.K., rensen, J. D.S., 2019. Probabilistic analysis of offshore wind turbines under extreme resonant response: Application of environmental contour method. Appl. Ocean Res. 93, 101947.
Volpi, E., Fiori, A., Grimaldi, S., Lombardo, F., Koutsoyiannis, D., 2019. Save hydrological observations! return period estimation without data decimation. J. Hydrol. 571, 782–792. https://doi.org/10.1016/j.jhydrol.2019.02.017
Wang, S., Moan, T., 2023. Serviceability limit state assessment of semi-submersible floating wind turbines. J. Offshore Mech. Arctic Engin. 146, 1–31. https://doi.org/10.1115/1.4063618
Wang, S., Moan, T., 2024. Methodology of load effect analysis and ultimate limit state design of semi-submersible hulls of floating wind turbines: With a focus on floater column design. Marine Struc. 93, 103526. https://doi.org/10.1016/j.marstruc.2023.103526
Wang, S., Moan, T., Gao, Z., 2023. Methodology for global structural load effect analysis of the semi-submersible hull of floating wind turbines under still water, wind, and wave loads. Marine Struc. 91, 103463. https://doi.org/10.1016/j.marstruc.2023.103463
Wilk, M.B., Gnanadesikan, R., 1968. Probability plotting methods for the analysis for the analysis of data. Biometrika 55, 1–17. https://doi.org/10.1093/biomet/55.1.1
Windeurope, 2025. Wind energy in europe: 2023 statistics and the outlook for 2024-2030. https://windeurope.org/intelligence-platform/product/wind-energy-in-europe-2023-statistics-and-the-outlook-for-2024-2030/.
Winterstein, S., Ude, T., Cornell, C., Bjerager, P., Haver, S., 1993. Environmental parameters for extreme response: inverse form with omission factors. In: Proc. of Intl. Conf. on Structural Safety and Reliability. ICOSSAR93.
Zachary, S., Feld, G., Ward, G., Wolfram, J., 1998. Multivariate extrapolation in the offshore environment. Appl. Ocean Res. 20, 273–295. https://doi.org/10.1016/S0141-1187(98)00027-3